

Jacquelyn Loven  
16 August 2017  
MSE 4000  
Final Report

## I. Abstract

Accurate measurement of hardness is a vital metric to understand deformation in glasses and therefore enable the creation of new glasses with improved resistance to surface damage. However, current methods to determine the area of indents in microindentation are prone to significant human error. The accuracy of this area value directly impacts the accuracy of a hardness calculation, so it is important for indent area measurements to be accurate and repeatable. Researchers conducting microindentation tests on metals have had success in using computer vision techniques to determine the size of indents from photographs, but photographs of glass indents prove difficult to analyze due to low contrast between indent edges and the surrounding glass surface. Thus, three methods of area determination are compared: confocal scanning laser microscopy (CLSM), atomic force microscopy (AFM), and a new method in which contrast of indent edges is increased by evaporating a layer<sup>1</sup> of Au-Pd onto indentations in glass. This final method is developed to require little time or instrument expense, in contrast to the other two methods, which require significant time and instrument expense. Samples are analyzed using tools available in proprietary software for the CLSM and AFM methods and indent areas are determined with code written using MATLAB's computer vision toolboxes, with data obtained from AFM serving as a standard. In the metallization method, samples are photographed and analyzed for indent areas with similar code. These three methods are developed and compared using indentations made in soda-lime silicate glass.

## II. Introduction

For widely used applications such as electronic displays and packaging, glasses need to have mechanical properties suitable for withstanding loads with minimal fracture and deformation. However, the deformation properties of oxide glasses are currently not well characterized. Currently, a common metric in the investigation of these properties is hardness, which is a measure for permanent deformation resistance under load. It is generally defined as the load used in indentation testing divided by the area of an indent created by an indenter tip of known geometry. A variety of common indenter geometries are used, and this area is measured differently for each.

The load as reported by microindentation machines has relatively low error<sup>2</sup>, but area measurements are often made using a subjective and error-prone technique [1]. Typically, users of a microindentation machine use a reticle to find the distance between pairs of opposing vertices of an imaged indent as shown in Fig. 1.

---

<sup>1</sup> This layer's composition and thickness will be determined in later experimentation.

<sup>2</sup> This error will be found in later experimentation.

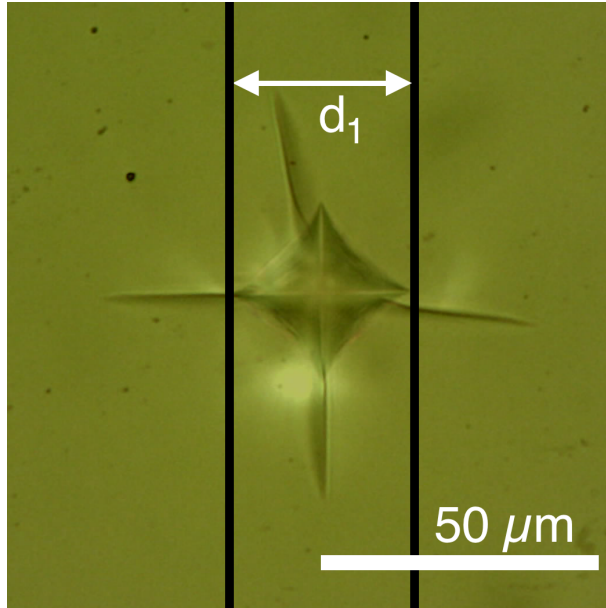
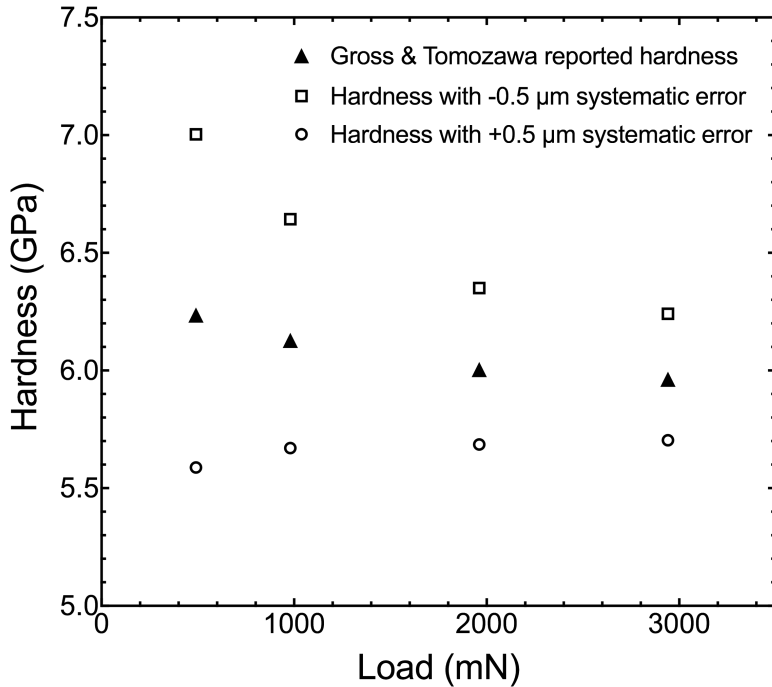


**Fig. 1:** The typical reticle method for microindentation hardness testing, as displayed for an indent in a soda-lime silicate glass imaged at 40x and created at a load of 2942 mN.

The Meyer hardness  $H$  is calculated from the applied load  $P$  divided by the projected area  $A$  which is found from the average  $d$  of the two diagonals  $d_1$  (shown in Fig. 1) and  $d_2$  assuming that the indent area is a square (Eq. 1).

$$H = \frac{P}{A} = \frac{P}{\frac{1}{2}d^2} \quad (1)$$

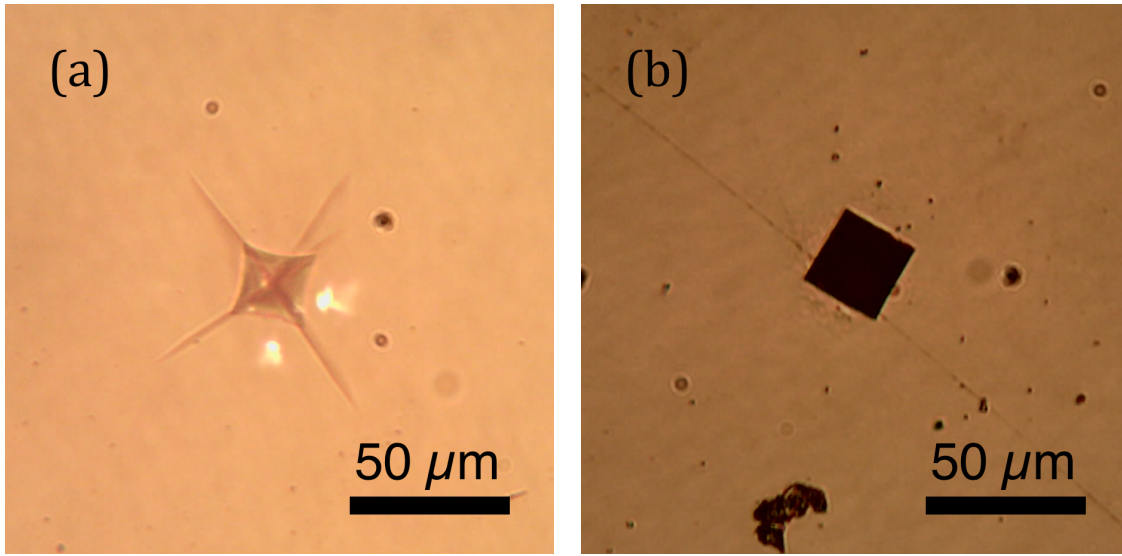
However, accurate determination of the distance between vertices of an indent can be difficult due to diffuse scattering and a lack of contrast introduced by subsurface cracks in glass. These characteristics of typical glass indentations contribute to poor contrast between indent edges and the glass surface, and can be further exacerbated by the irregular nature of indent boundaries when significant pileup is present. In the traditional reticle method, error arises in many aspects of the experiment. Operator judgment of the edges of an indent is chief among these, exacerbated by optical resolution of the imaging system and measurement reticle used. As shown in Fig. 2, when we apply a systematic error in reticle distance of just  $0.5 \mu\text{m}$  to data reported by Gross and Tomozawa, hardness measurements and the observed hardness vs. load trend change significantly [2].



**Fig. 2:** Gross and Tomozawa reported hardness data for a calcium aluminosilicate glass [2], but applying a systematic error of  $0.5 \mu\text{m}$  in the measurement of indent diagonals to their data would change the reported hardness trend.

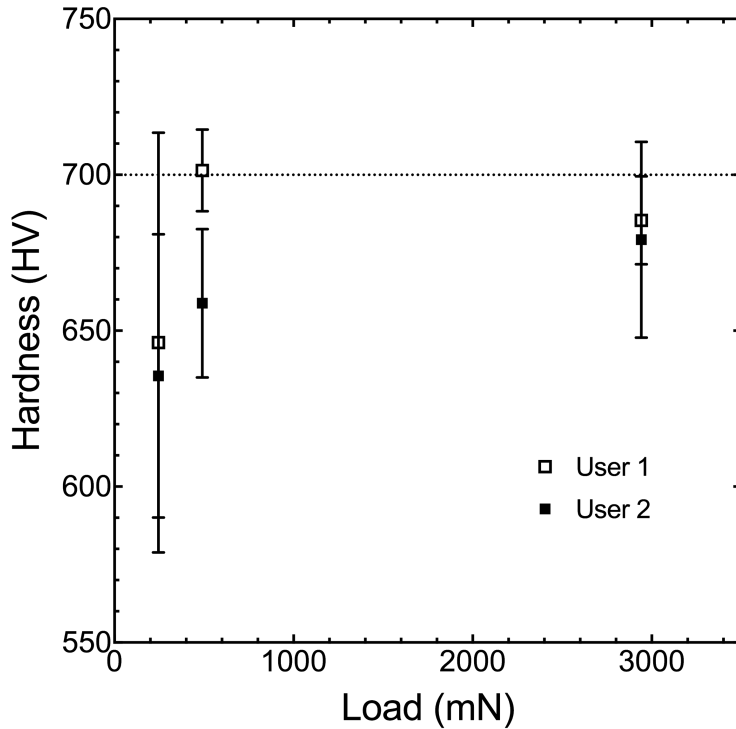
Furthermore, in the reticle method, different operators calibrate the measurement lines in a microindentation machine to a distance of  $0 \mu\text{m}$  differently, automatically resulting in different hardness measurements across experimenters. This recalibration is necessary because different users see the measurement lines and their displacement differently. We conducted measurements in which two different users of the microindentation machine calibrated the measurement lines to displacement of  $0 \mu\text{m}$  ten times, and just the calibration difference between users was  $0.12 \mu\text{m}$  (nearly a quarter of the systematic error shown to change hardness measurement trends as shown in Fig. 2). Furthermore, the standard deviation in reticle calibration for a single user was greater than  $0.06 \mu\text{m}$  for both users, or about 11% of the error shown to change hardness trends in Fig. 2.

Fig. 3(a) shows a typical glass indentation. The aforementioned phenomena that confound indent boundary determination are present, unlike for a typical indentation in metal, as shown in Fig. 3(b).



**Fig. 3:** Images at 20x magnification of (a) an indentation in glass at load 2942 mN (b) an indentation of comparable size in a 700 HV metal standard

In addition to the already poor contrast seen in glass indentations, human judgment in measurement of indent diagonal lengths can contribute significantly to error. Each user of a microindentation machine may determine the area of an indent in a different manner even if the machine is calibrated the same for both users. We collected hardness data using a 700 HV metal standard (Standardized Block for Hardness 700 HV, Aioi Hyogo Japan) with two different users but with the same calibration. As shown in Fig. 4, hardness data collected by one user deviates significantly both from the reference value of 700 HV and from the data collected by another user. Researchers may even find opposite trends in hardness vs. indentation load for a given set of samples [1]. There are reports of both an indentation size effect (where measured hardness decreases with applied load) [3-10] and a reverse indentation size effect [11] in current literature.



**Fig. 4:** Vickers hardness data gathered on a 700 HV sample gathered by two different users for four indents at each of the three loads. At a given load, error bars represent the standard deviation for each user's measurement of four indents.

Finally, optical methods have an inherent resolution limit due to the wavelength of light; in the systems used for this research with objective numerical apertures of 0.45 and 0.65 the smallest optically discernible features are approximately 528 nm and 392 nm, respectively (Metallux 3, Leitz Wetzlar; HWM-MT-X3, Nanovea) assuming blue light ( $\lambda \approx 475$  nm) provides the best resolution for the former and when a green light filter ( $\lambda \approx 510$  nm) is used for the latter. Therefore, this error alone has the potential to be equal to or even greater than the error of 500 nm needed to significantly alter a trend seen in hardness values, as shown in Fig. 2. Thus, while the reticle method is fast and widely available in hardness testing research, the compounding error from user calibration, user discretion in indent diagonal measurement, and optical resolution is prohibitive in the gathering of meaningful data.

### *Area Definitions*

In addition, the definition of which area to measure in microhardness testing is not universal, and the assumption that Vickers indents are square is not accurate in many cases. Meyer hardness, as defined above, is the quotient of the load used and a measurement of the projected area of an indentation. This is the area of the indentation which intersects the plane of the material's surface. In Vickers hardness measurements, the residual area of indentations is the surface area of the material that is in contact with the indenter. The load used is divided by this contact area to

obtain a Vickers hardness value. In nanoindentation testing, the depth of a tip of known geometry is precisely monitored, and the residual area of an indentation is calculated using the value of the depth achieved during the indentation experiment and the tip geometry [12].

However, as described above, the measurement of these hardness values typically involves the assumptions that a) indents are square and b) that the measurement of both indent diagonals is sufficient to represent the square area. In reality, a pincushion effect is seen in measurements of glass hardness [13], in which the indent is seen to be closer to the shape of an astroid than a square. Thus, Meyer and Vickers hardness data based on diagonal averages is inherently inaccurate.

Based on the degree of pincushioning, we calculated the change in the projected area and therefore the Meyer's hardness, assuming that indentation edges are circular arcs as shown in Fig. 5. Using the variables defined in Fig. 5 (b), the area of the indentation is calculated as the square created by the area  $1/2d^2$  with total the area of four circle segments subtracted, as shown in Eq. 1. In the limit  $r=2d$ , pincushion projected areas deviate from square projected areas by 58%.<sup>3</sup>

To better understand how Vickers hardness is affected by pincushioning, we would want to calculate the deviation from a square pyramid. However, we cannot assume a 3 dimensional version of the astroid shape because the half diagonal is much larger than the depth of the residual indentation from a shallow indenter like Vickers, which indicates that the z dimension is smaller than the x and y dimensions.

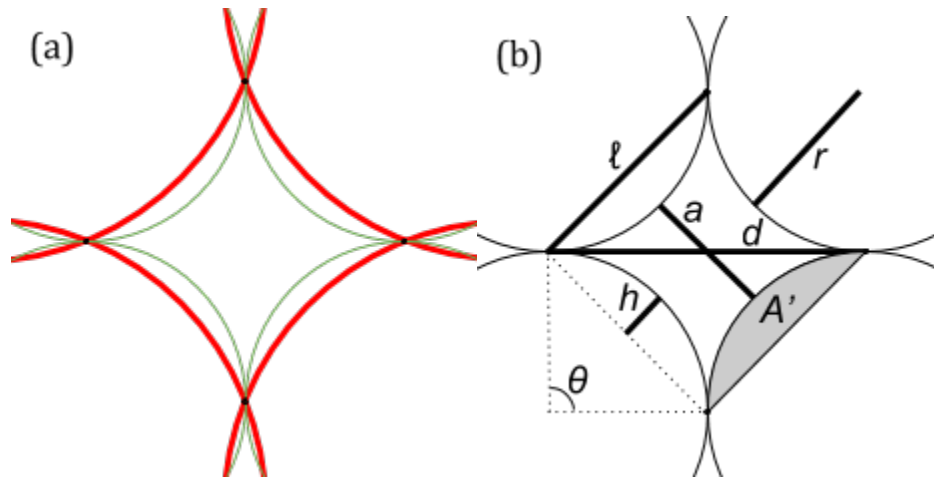


**Fig. 5:** (a) Demonstration of two possible degrees of pincushioning. The bolded red lines represent circles that produce an indent with a moderate degree of pincushioning with a radius of  $R$ . The narrow green lines represent circles that produce an indent with the maximum possible pincushioning (following a model where the indentation edges are assumed to follow segments of circles) where the radius  $R' = \frac{1}{2}d < R$  where  $d$  is the indent diagonal. (b) Schematic of the variables necessary to determine the extent of pincushioning.  $d$  is the diagonal,  $a$  is the face to face distance,  $\ell$  is the length of the chord defining the circle segment,  $h$  is the height of the circle segment,  $\theta$  is the angle that subtends the circle chord along the edge of the indent,  $r$  is the radius of the circles that form the indent,  $A'$  is the area of the circle segment.

---

<sup>3</sup> This derivation will be shown in later versions of this work.

Furthermore, pileup around the edges of indents confounds contact area measurements, because it is possible that the indenter remained in contact with the material at points on the pileup above the surface of the surrounding glass [13]. Therefore, measuring contact area at the plane of the material's surface without considering pileup does not encompass the true contact area between the indenter and the material.

### *Indentation Test Analysis Methods*

In current literature, the dependence of plastic deformation in glass with regard to load in microindentation and systematic compositional variation has not been widely studied. However, in order to characterize the indentation properties of large ranges of glass composition and gather enough statistics for comparison, a repeatable and high-throughput method is needed. Furthermore, new methods are needed to mitigate the significant error inherent in current microindentation tests.

Past research by others has resulted in methods for indentation image analysis, but these methods are not available to the general scientific community due to cost, restrictions on compatible microindenter machines, and requirements for the contrast of gathered images. Previously, groups have created software in MATLAB and C++ using standard image processing techniques to detect indentation sizes in high-contrast images in metals [14-16]. However, their results were obtained from indent images with much higher contrast than images taken in the present work. We attempted to use these programs to analyze indentations in glass, but the poor contrast seen in glass prevented the software created during these previous studies for metals from accurately identifying indent areas in glass. The basic noise reduction techniques used served as a starting point for this research.

Currently, the reticle method is the most widely available method to indentation hardness researchers. Data collection using this method is fast but not accurate or precise due to significant human error, and the inability to account for pincushioning and pileup. In the present work, we examined several methods to remedy this error.

The first method involved the use of CLSM to image indents. A confocal laser scanning microscope creates a 3 dimensional image of a sample's surface topography by combining a series of images acquired at different depths. At the depth of the glass surface that is not indented, the indent residual area can be identified as a hole in the surface scan. CLSM limited the slight chromatic aberration seen in optical microscopy that could cause difficulty in determining the locations of diffuse indent edges and provided an accurate depth measurement of indents so that it was simple to determine where the glass surface plane intersected indent edges. However, CLSM was not as precise as other profilometry techniques like AFM, necessitated the use of an instrument that may not be commonly available in hardness testing laboratories, and increased the indent analysis time over the reticle method.

Thus, we created a method for indent area detection in glasses that involved no uncommon instruments and required just an optical microscope, camera, and

metal sputterer. We coated glass indents with a layer of metal to increase their contrast in optical microscopy. Then, we photographed these metallized indents and wrote image analysis software to report indent areas. This method precluded the need for a human observer to measure area and added only the time needed to sputter a thin metal coating onto samples. Thus, we produced a repeatable, precise optical microscopy method for indentation test analysis.

We compared data from the laser profiler and from metallization to data from AFM measurements. The main advantage of AFM is that it provides a direct measure for surface topography, ensuring that scans were as close to reality as possible. In this method, we selected the area of indents at the height of the surrounding glass surface and wrote software to calculate the residual areas. However, AFM is significantly time consuming, and may not be feasible for the analysis of many indents. Thus, this analysis functioned to ensure the reliability of the new metallization method.

### III. Experiments, Analysis, and Results

We stored soda-lime silicate microscope slides of dimensions 75 x 25 x 0.96-1.06 mm (2947-75x25, Corning, Inc.) between 51% and 57% humidity at temperatures between 22°C and 23°C for more than one day. Following repeated washing with acetone and then isopropyl alcohol and drying by air, we used the samples for Vickers microindentation (HWM-MT-X3, Nanovea). We made four indentations each using loads of 245.2 mN, 490.3 mN, and 2942 mN with a 15 s dwell time. We obtained images of indentations at 40x magnification under filtered green light (HWM-MT-X3, Nanovea; Dino-Lite AM7025X, AnMo Electronics Corp.).

#### CLSM

##### (1) Experiment

We used a confocal laser scanning microscope (VK-X260K, Keyence Corp.) with laser wavelength 408 nm to measure indent areas at 100x magnification. The reported resolution of the laser profiler is 0.2  $\mu\text{m}$  laterally and 5 nm vertically, but due to vibrations and thermal noise this precision was never achieved with the current laser profiler setup<sup>4</sup>. We imaged indents with the laser profiler's "Auto" setting, in which the determination of the height range to image is automatic.

##### (2) Raw Results

An image of an indent as measured with CLSM is shown in Fig. 6.

---

<sup>4</sup> The actual precision will be determined in later experimentation with profiles of a CLSM standard.

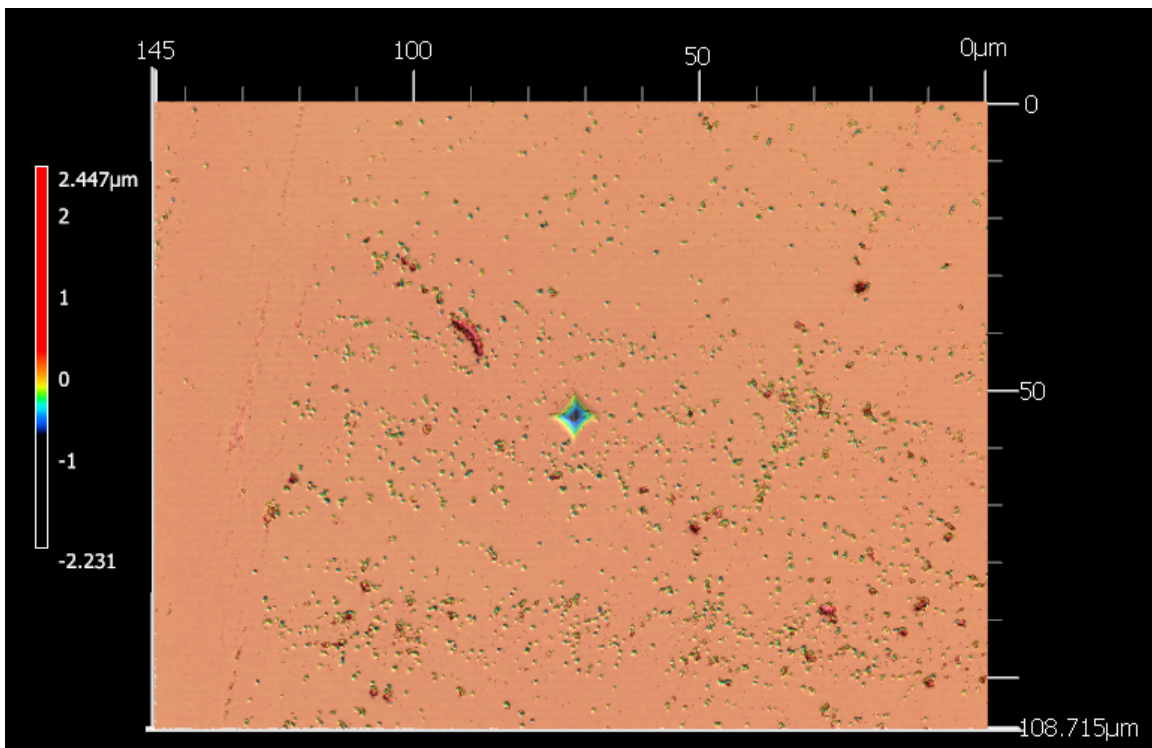


**Fig. 6:** A height profile of an indent created at a load of 245.2 mN as measured by the CLSM.

### (3) Analysis

Based on the assumption that the intersection of a plane fit to the sample surface with the 3 dimensional profile would give accurate area measurements, we batch-processed laser profiler scans in the provided software (MultiFileAnalyzer 1.3.1.120, Keyence Corp.) to determine the size of residual areas. We preprocessed each image by excluding a rectangle surrounding the indent area, creating a plane fit, and using this plane fit to level the entire measured surface. Then, we selected a rectangular area larger than the indent but not encompassing the entire measured surface for analysis. We selected this area in black, and the software used the previously calculated plane to select all surfaces below this threshold in green. We ignored any selected areas that were not in direct contact with the area of the indent. We used the projected size of the green pincushioned area calculated by the laser profiler software (Fig. 7) as the “C.S. Area” (cross-sectional area, or the size of the indent hole) in analyses. We also determined the area of each indent using the Vickers assumption that the indent is square by measuring the average diagonal length. We wrote software that allows a user to select the outermost green pixel on each of four indent corners for each indent (see Appendix), and the software computes an area based on the size of the image’s scale bar. For the largest load, all indent images from CLSM included cracks, so operator judgment was used to determine indent vertices. Diagonal lengths are displayed in Fig. 8.

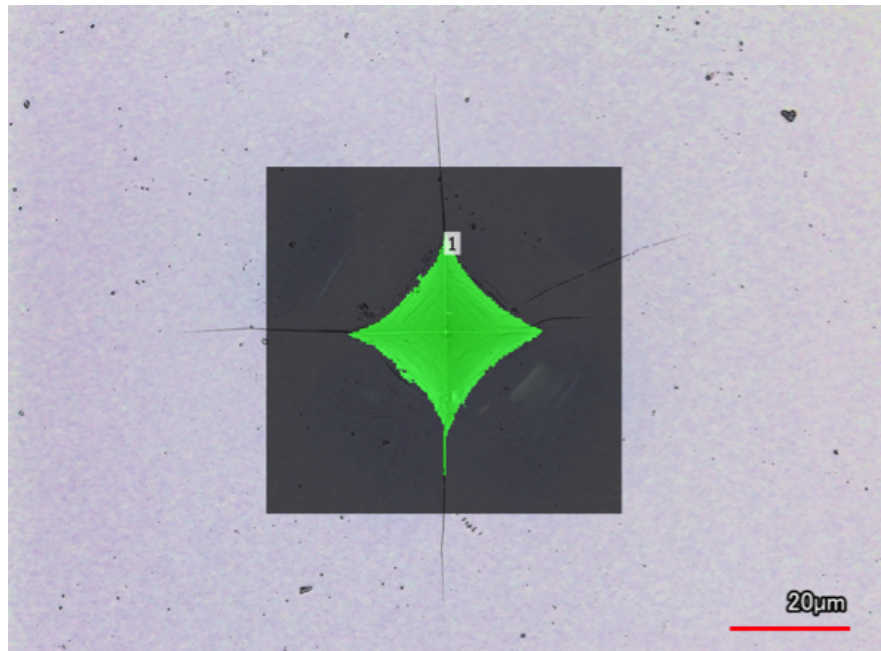


**Fig. 7:** An indent created with a load of 2942 mN with pincushioned area masked in green over a combination of laser and optical images.

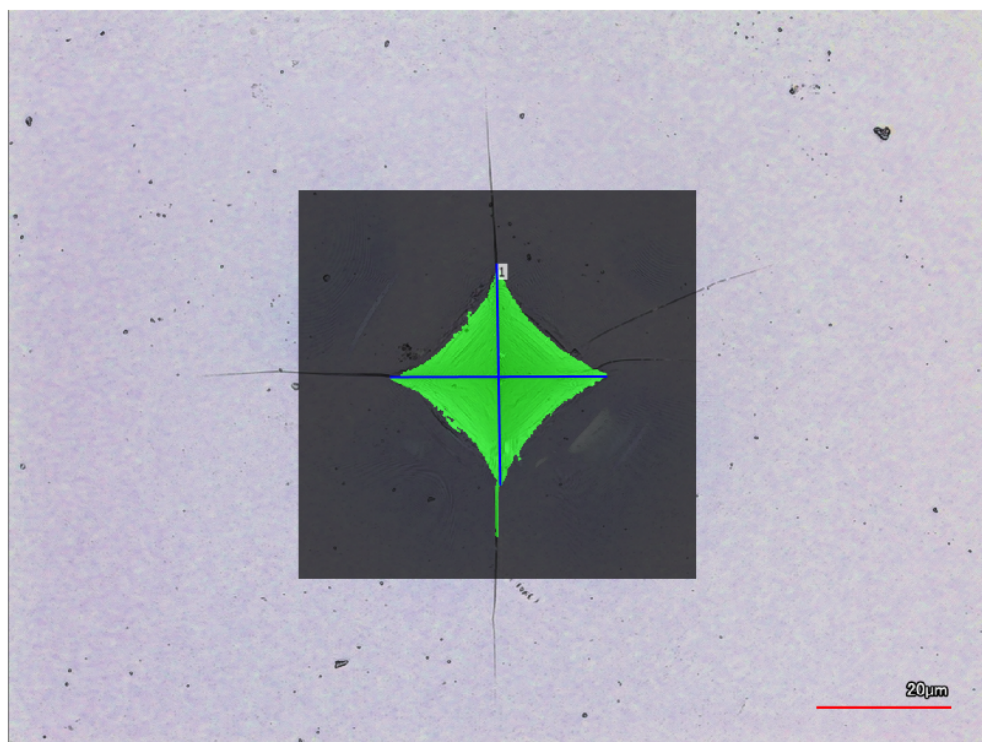


**Fig. 8:** The same indent from Fig. 7 with diagonal lengths (with operator judgment to exclude a crack) shown in blue.

#### (4) Final Results

As shown in Fig. 16, the average hardnesses as calculated by the CLSM method ranged between  $6.2 \pm 0.5$  GPa at the lowest load and  $7.6 \pm 0.1$  GPa at the highest load, and hardness increased with load. The hardness calculated using the measurement of average diagonal length ranged between  $5.2 \pm 0.3$  GPa and  $5.6 \pm 0.2$  GPa (Fig. 17).

### AFM

#### (1) Experiment

We used AFM (MFP3D-Bio-AFM-SPM, Asylum Research) in contact mode with silicon nitride tips of spring constant 0.006 N/m (BL-RC150VB, Olympus Corp.), and conducted scans at a rate of 0.5 Hz over squares of width approximately 10  $\mu\text{m}$  for the smallest (245.2 mN) indents to approximately 40  $\mu\text{m}$  for the largest (2942 mN) indents. The reported resolution of the AFM is laterally 5 Å and vertically 0.6 Å.

#### (2) Raw Results

An image of an indent as measured with AFM is shown in Fig. 9.

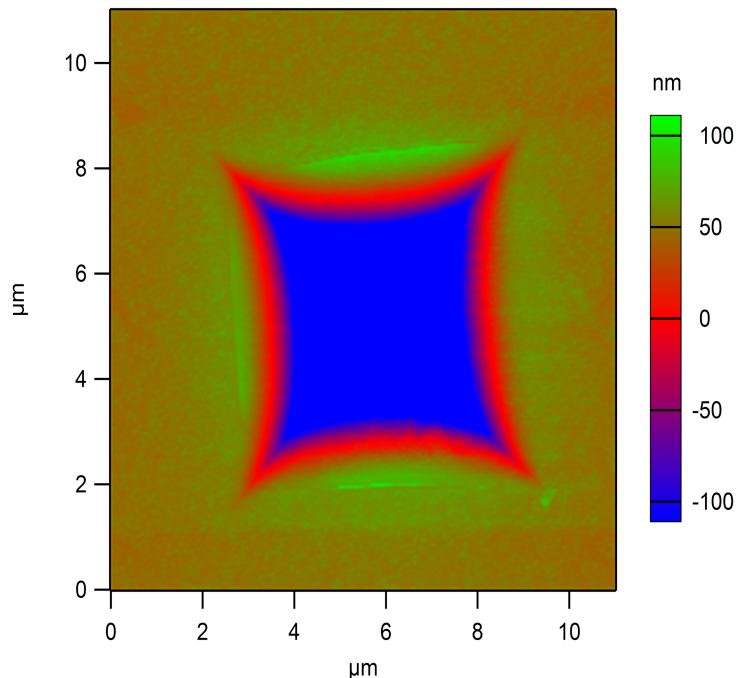


**Fig. 9:** A height profile of a sample indent created at load 245.2 mN as measured by AFM<sup>5</sup>.

<sup>5</sup> The proprietary software does not allow a larger range of heights to be mapped without losing definition, and as such, slightly over 200 nm are mapped in this color map.

### (3) Analysis

We leveled indent images from the AFM z-sensor by fitting a first-order polynomial to each AFM line scan and subtracting it from the raw data with the indent area masked (Igor Pro 6.3.7.2, Asylum Research). We then selected pincushioned indent area by choosing a height threshold such that the entirety of the indent astroid shape was distinct from other features detected on the glass surface by at least several pixels (Fig. 10). We calculated the indent area resulting from an opaque red mask of this threshold (Fig. 11 (a)) using MATLAB code that we wrote to determine the number of masked pixels inside the indent (the largest masked feature). To translate between the number of pixels and the true area in square microns, we wrote code to allow a user to select five consecutive scale bar markings in each AFM image and input their distance apart in microns. The average distance between these markings was used as a metric for microns per pixel (see Appendix). The final pincushioned area is shown in Fig. 11 (b). We also computed the area of each indent using the aforementioned software that we wrote to determine indent diagonal lengths (see Appendix). Diagonal lengths are displayed in Fig. 12.

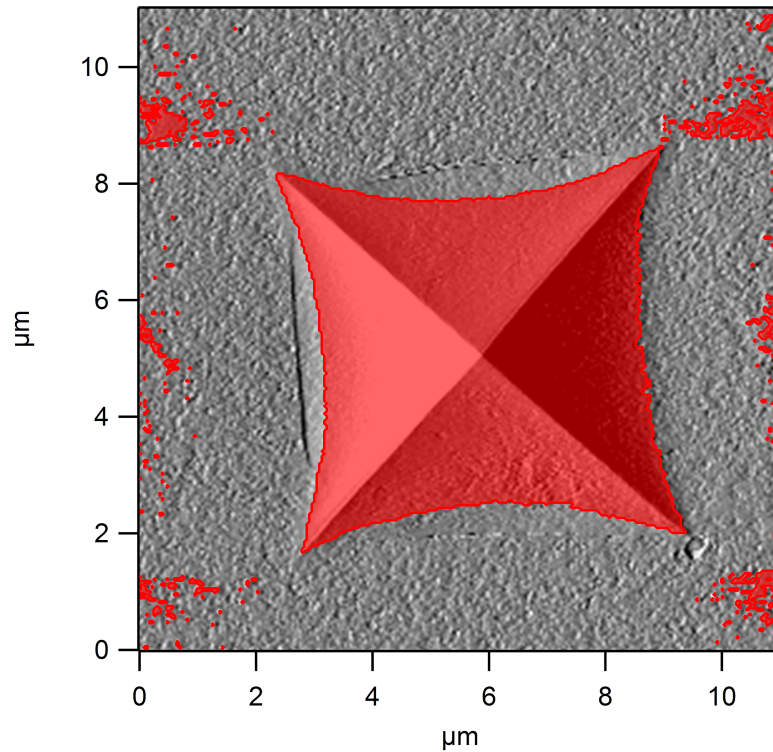


**Fig. 10:** The same indent shown in Fig. 9 with the pincushioned area below the chosen height threshold selected in a red translucent mask for easy viewing of indent edges under the mask. This mask was selected using the AFM z-sensor and copied to a deflection scan for illustration purposes.

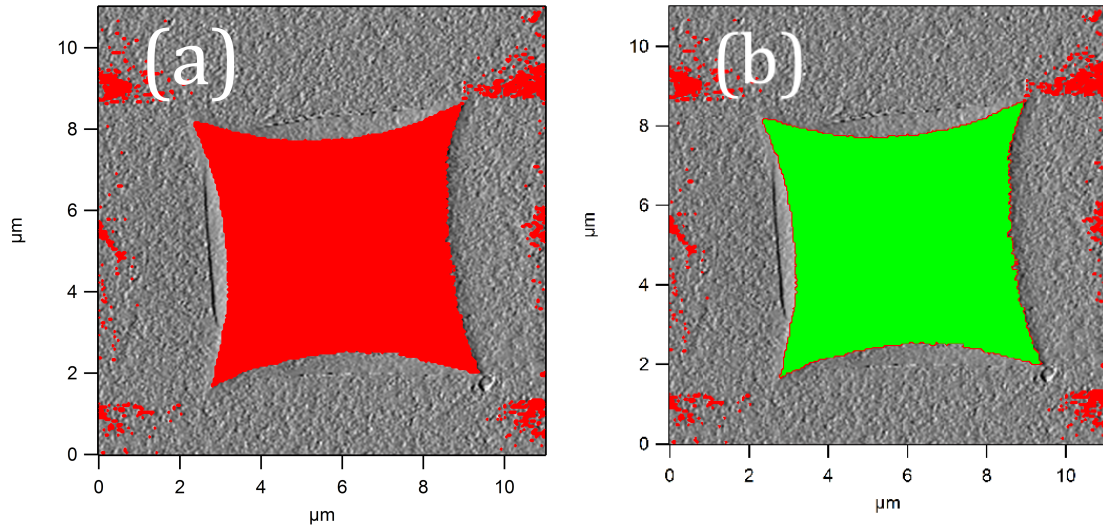


**Fig. 11:** (a) The same indent shown in Fig. 9 with an opaque mask needed for the MATLAB software we wrote to determine indent size. (b) The indent area masked in green.

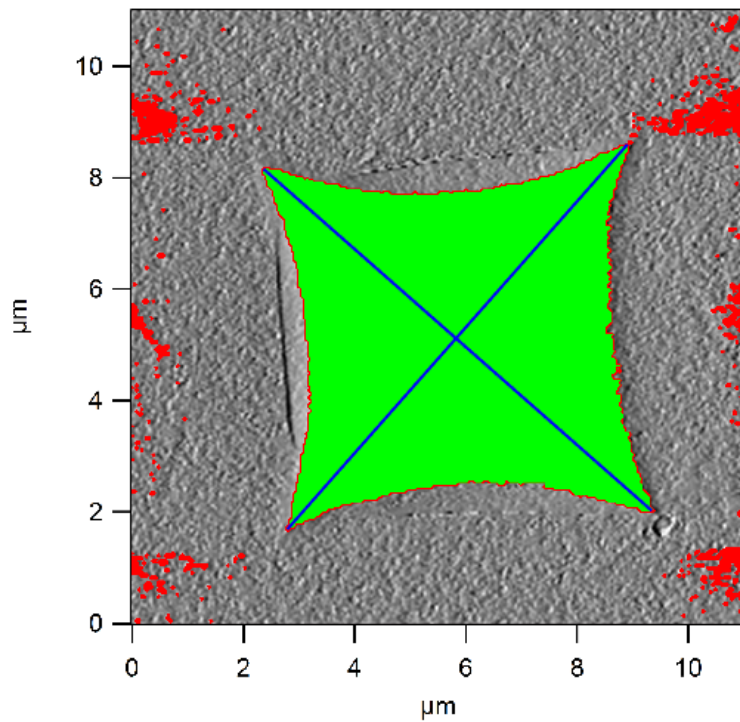


**Fig. 12:** The same indent from Fig. 11 (b) with diagonal lengths shown in blue.

#### (4) Final Results

As shown in Fig. 16, the average hardnesses as calculated by the AFM pincushion analysis ranged between  $7.1 \pm 0.3$  GPa at the highest load and  $7.4 \pm 0.2$  GPa at the lowest load. Hardness decreased with load. The hardness calculated using

the measurement of average diagonal length was  $5.5 \pm 0.2$  GPa and was constant with load (Fig. 17).

### *Metallization*

#### *(1) Experiment*

In the metallization method, we masked the indented glass slides on the indented surface far from the indents with Kapton tape (to produce a measurable step edge) and sputter coated them with a layer of Au-Pd<sup>6</sup> (Desk V, Denton Vacuum) while rotating them for 240 seconds in a vacuum of at least  $6 \times 10^{-4}$  Torr with a 30 mA DC current set point. We imaged the metallized samples at 20x magnification with the aperture diaphragm fully closed down (Metallux 3, Leitz Wetzlar; Dino-Lite AM7025X, AnMo Electronics Corp.).

#### *(2) Raw Results*

The optical contrast difference between a typical glass indentation and its metallized glass counterpart under the same microscope settings is shown in Fig. 13 (a) and (b).

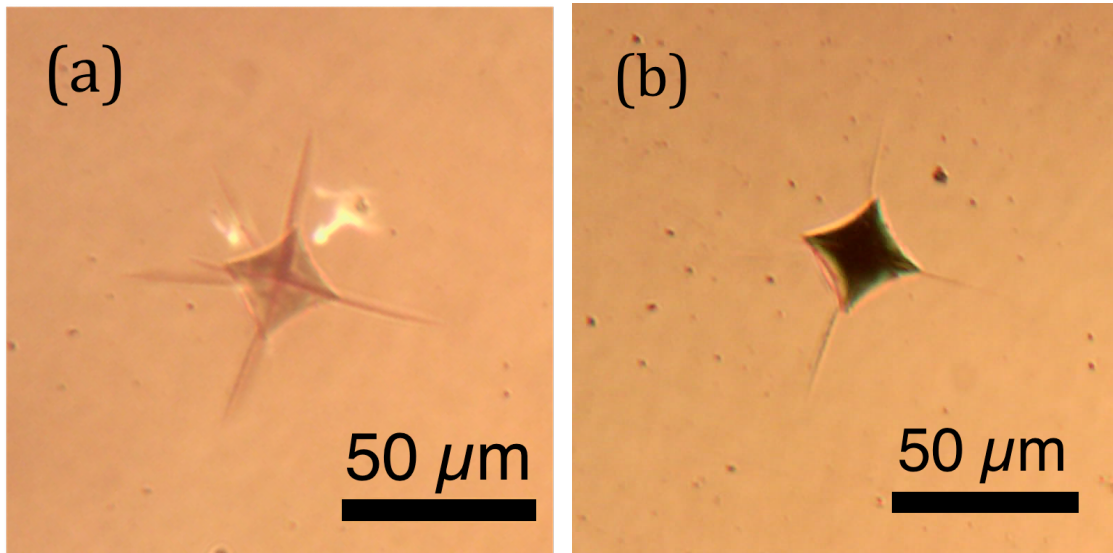


**Fig. 13:** (a) A glass indent created at load 2942 mN imaged at 20x, (b) the same indent imaged under the same conditions after metallization.

#### *(3) Analysis*

We wrote software to detect indent sizes from images of metallized glass samples (MATLAB R2017a with Image Processing Toolbox 10.0 and Computer

---

<sup>6</sup> This layer's composition and thickness will be determined in later experimentation.

Vision System Toolbox 7.3, MathWorks). We used the image processing techniques of gray scale conversion, erosion, dilation, adaptive binarization, Canny edge detection, and contour searching by area to write software to determine indent areas. These operations were used to reduce noise in images from particulate matter and metal coating irregularities. In the written software, a user selects the locations of five consecutive markings in a photographed reticle to allow the software to convert pixel areas to areas in square microns. Fig. 14 shows the area identified by the software we wrote (see Appendix) to accompany the metallization method. We also computed the area of each indent using the aforementioned software that we wrote to determine indent diagonal lengths (see Appendix). Diagonal lengths are displayed in Fig. 15.

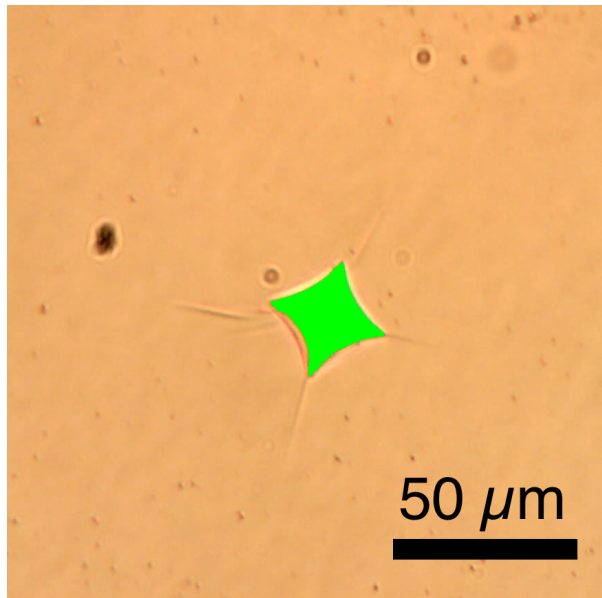


**Fig. 14:** A sample indent as measured by the metallization method, with indent area masked in green.

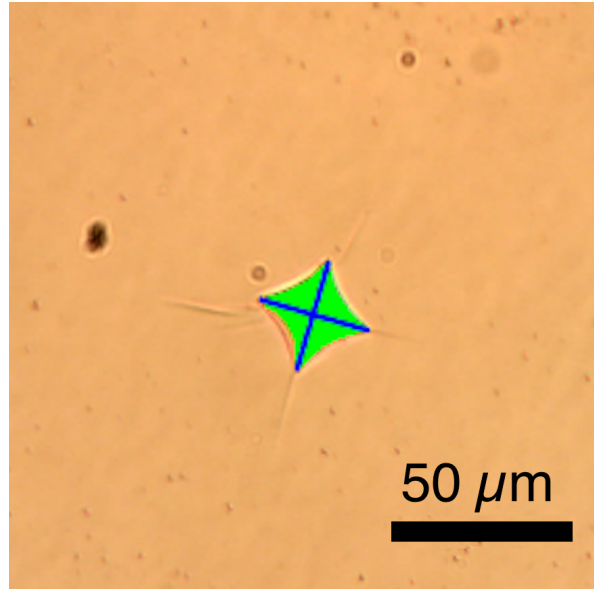


**Fig. 15:** The same indent from Fig. 14, with diagonal lengths shown in blue.

#### (4) Final Results

As shown in Fig. 16, the average hardnesses as calculated by the metallization method ranged between  $6.9 \pm 0.5$  GPa at the middle load and  $7.9 \pm 0.2$  GPa at the highest load. The hardness calculated using the measurement of average diagonal length ranged between  $5.78 \pm 0.08$  GPa at the largest load and  $7.31 \pm 0.05$  (Fig. 17), and decreased with load.

#### Summary

Area results from three hardness analysis methods are summarized in Table 1, and average hardness values for each load and method are shown in Fig. 16. Uncertainty in load values is assumed to be smaller than the symbol size.

**Table 1:** Average area results for the three different methods.

| Load  | Laser Profiler<br>Average Area<br>(Pincushioned) | Laser<br>Profiler<br>Average Area<br>(Square) | AFM Average<br>Area<br>(Pincushioned) | AFM<br>Average<br>Area<br>(Square) | Metallization<br>Average Area<br>(Pincushioned) | Metallization<br>Average Area<br>(Square) |
|-------|--|---|---------------------------------------|------------------------------------|---|---|
| [mN]  | [μm <sup>2</sup> ]                               | [μm <sup>2</sup> ]                            | [μm <sup>2</sup> ]                    | [μm <sup>2</sup> ]                 | [μm <sup>2</sup> ]                              | [μm <sup>2</sup> ]                        |
| 245.2 | $39.0 \pm 3.0$                                   | $44.9 \pm 0.9$                                | $33.0 \pm 0.8$                        | $45 \pm 1$                         | $34.9 \pm 0.7$                                  | $33.6 \pm 0.2$                            |
| 490.3 | $76 \pm 5$                                       | $95 \pm 5$                                    | $66.1 \pm 0.9$                        | $89 \pm 4$                         | $71 \pm 5$                                      | $74 \pm 2$                                |
| 2942  | $386 \pm 7$                                      | $520 \pm 15$                                  | $420 \pm 19$                          | $540 \pm 16$                       | $371 \pm 9$                                     | $509 \pm 7$                               |

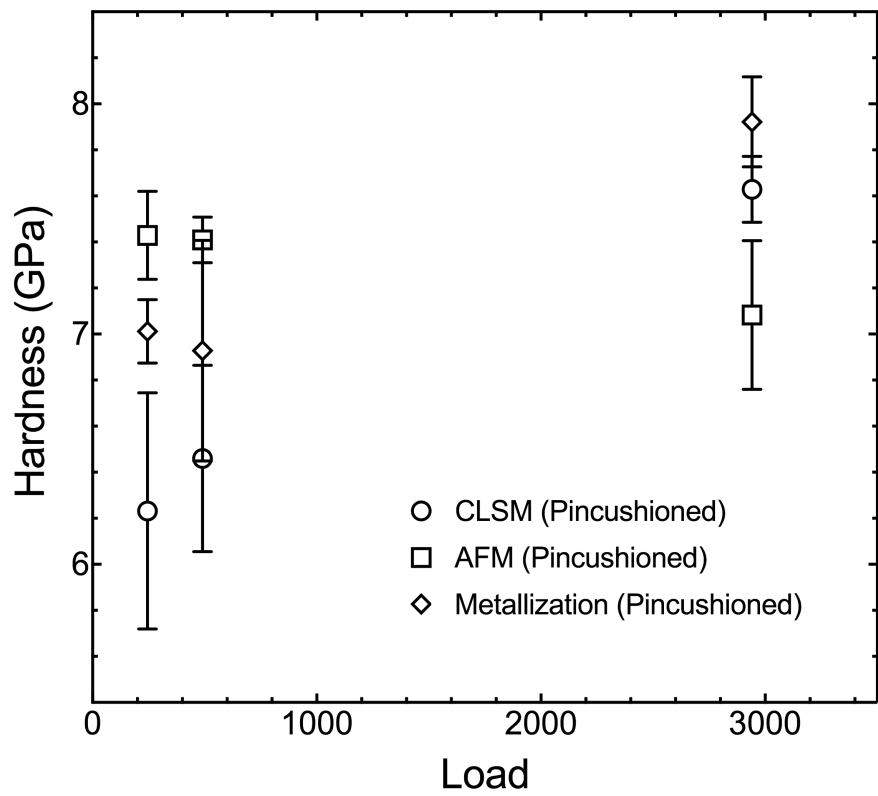


**Fig. 16:** Average pincushioned hardness values for each load and method as reported in Meyer hardness.

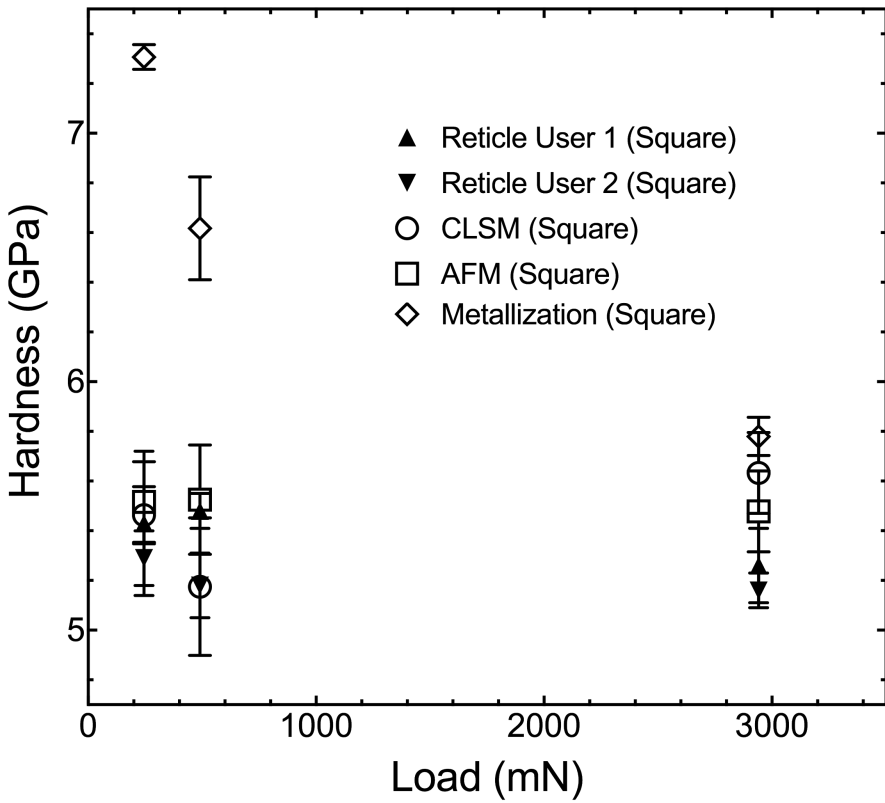


**Fig. 17:** Average hardness values, under the assumption that indents are square, for each load and method as reported in Meyer hardness.

#### IV. Discussion

In the present work, we developed several repeatable methods for indentation hardness analysis. Unlike the reticle method, different users can utilize the AFM, CLSM, and metallization methods that we developed at different times and achieve the same results. However, each of the methods produced dissimilar hardness values despite measuring the same indents. Thus, while the methods are repeatable, it is not possible to tell which, if any, are accurate. The difference in hardness values between the AFM and CLSM methods could be due to a lack of adequate depth calibration in both: the AFM was calibrated on a step edge that was an order of magnitude smaller than any indent measured<sup>7</sup>, and the laser profiler was calibrated only on an optical flat. Furthermore, because indents were analyzed using proprietary software in the AFM and CLSM methods, it is possible that different height thresholds were used in each method. We found that for small indents where a height threshold change more significantly changes the measured area, a height threshold change of -40 nm from the surface resulted in a hardness change of 2 GPa for AFM and 1 GPa for CLSM (Fig. 18). This change, while less

---

<sup>7</sup> The AFM will be calibrated on a 4.8  $\mu\text{m}$  step edge in further experimentation

significant for larger indents, is still over 5% for both methods. Any indent without enough height contrast to show a discernible shape (similar to an astroid) was not considered in the data analysis, because moving the height threshold down by any amount to increase this contrast altered the measured area significantly. This limited the smallest analyzable indent to one created under a load of 245.2 mN for CLSM.

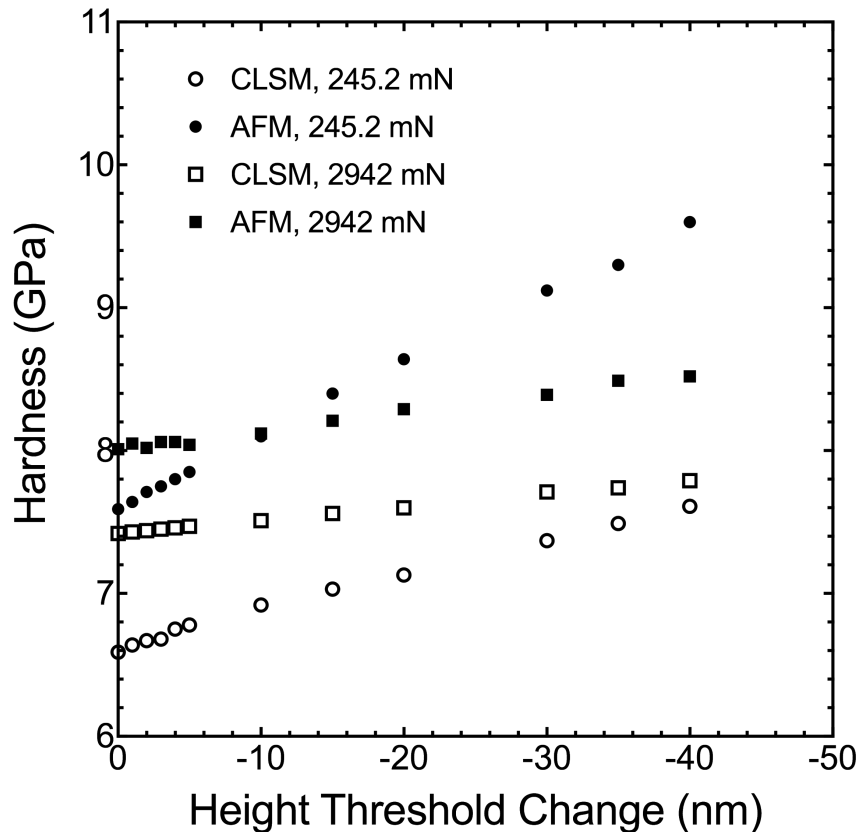


**Fig. 18:** Changing the height threshold at which to measure indent area in CLSM and AFM changes the measured area. One indent was analyzed per load and the same indent was imaged with the laser profiler and AFM.<sup>8</sup>

As discussed in the Introduction, an indentation size effect is prevalent in glass hardness research. However, due to the spread in data collected in the present work (Figs. 16 and 17), it is not possible to conclusively determine the presence of such an effect.

AFM data acquired via the square approximation were taken as the standard because they represented the most direct measure and replicated common measurements via the reticle method. CLSM and metallization data underestimate material hardness for small loads and overestimate hardness for large loads. The standard deviations in area measurements were under 8.3% of average values for all loads and methods.

---

<sup>8</sup> This analysis will be done for positive height threshold choices in later experimentation.

Values obtained with the square approximation are most commonly reported in current literature because of the proliferation of the reticle method. Data collected in the present work are within the large range of hardness values reported for soda-lime silicate glasses (3.11 GPa to 6.87 GPa [10, 17-25]), but metallization values under the square approximation and pincushion hardness values lie above this range. In the metallization method, image processing techniques used to reduce noise also reduce definition in small features such as indent corners. Thus, any diagonal measurements in this method underestimate the true diagonal measurements, resulting in an artificially high hardness (Fig. 17) for indents approximated as squares. The discrepancy between hardness values obtained from indents treated as pincushions and indents treated as squares is because pincushion areas are defined differently from square areas. Pincushion areas can be significantly smaller than square areas, as shown in Fig. 5, thus leading to much higher calculated hardness values.

In the CLSM method, laser profiler measurements often included area found in cracks with the indent area, as shown in Fig. 7. These extra areas were not cropped out to ensure that human judgement did not alter measured areas, and this caused an overestimation of area for some indents. This systematic overestimation of area should lead to an underestimation of hardness and is consistent with the pincushioned data shown in Fig. 18, because CLSM hardness values are lower than AFM hardness values. However, at the highest load (Fig. 16), CLSM hardness values are greater than AFM hardness values, and this is inconsistent with the source of error in crack area<sup>9</sup>. Overall, the incorporation of computer analysis in this method provided the repeatability that the reticle method lacks. However, because of the drawbacks of the necessity of an extra instrument and more analysis time, this method was not ideal.

AFM is recognized to be the most direct method for measuring surface topography with the least amount of error. We used contact mode AFM to lessen error related to the depth of indents (large depths of greater than a few microns measured in air may be negatively affected by damping in tapping mode), but similarly to the laser profiler method, the decision of which height threshold should determine the indent area introduces error, as shown in Fig. 18. While this method provided the most accurate topography data, it was prohibitively time consuming for experiments involving many indents and many samples.

In both the AFM and CLSM methods, error arises from the assumption that the glass surface surrounding the indent is flat. Surface features and dust can skew the plane fit, impacting the area measured at the plane's height threshold. If the majority of the scan size in an image contains the indent and not surrounding glass, such surface features can also easily skew the plane fit and change the area measured. These errors are similar in nature to the error caused by an indenter tip that is not mounted perpendicular to the surface: the indent size will not be measured correctly due to an incorrect choice for threshold plane. To mitigate the errors associated with threshold plane choice, another possible technique for indent area size analysis involves using two corner-to-corner line scans. While eliminating

---

<sup>9</sup> This inconsistency will be investigated in further experimentation.

the aforementioned surface-related errors, this method reintroduces the assumption that indents are square and requires precision in locating opposing corners of the indent. Furthermore, pileup around indentation would obfuscate the determination of the diagonals and force another assumption to be made about how much pileup should be considered in the diagonal distance. Including the pileup would increase the diagonal distance and thus increase the area.

Errors introduced in the image analysis software for the metallization technique primarily arise from image sharpness, mitigated through the use of a 5 MP camera and the use of image processing techniques to produce a low-noise image that is high contrast in all areas. However, the maximum resolution of images collected was the size of one pixel, measured to be  $186.94 \pm 0.08$  nm. Additionally, the error inherent in optical techniques as discussed in the Introduction is also present in the metallization method. We mitigated error in length measurements through the repeated selection of several markings in a photograph of a reticle. In this method, it was imperative that the user maintains the same focus when collecting all images across a test, ensured by focusing on small surface features nearby the indent in each image. This method produced data much closer to AFM data than the laser profiler method, was significantly less time consuming than both AFM and CLSM, and had the advantage that an image of an indent would be analyzed the same way regardless of user. Thus, we deemed it a repeatable, feasible method for the analysis of many microindentations in glass.

## V. Conclusions

Several different methods for glass microindentation hardness evaluation analysis were characterized. The commonly used reticle method incurs too much error to provide meaningful results. AFM, while providing the most accurate topography data, is prohibitively slow for the analysis of many indents. CLSM provides repeatable results but adds time and instrument costs to hardness measurement analysis. A simple method involving a metal coating on glass indents provides repeatable results more similar to AFM data than CLSM, and adds a negligible amount of time to data analysis. However, because none of the methods provided consensus results on soda-lime silicate glass hardness, none could be proven accurate. Thus, the CLSM, AFM, and metallization methods ensure more repeatable data analysis through the incorporation of computation, but do not necessarily provide accurate results. Future work in this area includes the further investigation of error in the aforementioned methods, and the refinement of a method to accurately characterize the deformation properties of a wide range of glass compositions under a large range of loads.

## VI. Appendix

Code for determining the size of indent areas and indent diagonals from AFM masked images can be found at [https://github.com/jLoven/hardness\\_test\\_area\\_detection/blob/master/matlab/find\\_AF\\_Masked\\_area.m](https://github.com/jLoven/hardness_test_area_detection/blob/master/matlab/find_AF_Masked_area.m). The user can input the file paths (any standard image file

format is accepted in MATLAB's imread function) of a masked AFM scan. First, a user clicks five consecutive points on the scale bar in the AFM image and inputs the distance between these points. The software determines an average number of pixels per input metric. Then, it determines the number of red pixels in the largest feature in the AFM image. It does this by scanning over every pixel in the image, copying the red pixels as white pixels onto a blank black image of the same size (to increase contrast) and counting the number of pixels in the largest contour found. These pixels are shown as green on the original image to allow the user to view the determined area. Finally, the software converts the pixel area to an area in square microns using the calculated conversion factor. Once the green area is displayed to the user, the software prompts the user to zoom in on and select the outermost green pixel on each indent in a clockwise fashion. Given these pixel locations and the already calculated length conversion factor, the software calculates two diagonal lengths and their average. The square area of the indent is calculated from this diagonal value.

The indent diagonal measurement code and code for selecting reticle size from this file is also used for the analysis of CLSM masked images.

Code for determining the size of indent areas from high contrast images of metallized glass can be found at [https://github.com/jLoven/hardness\\_test\\_area\\_detection/blob/master/matlab/indent\\_identifier.m](https://github.com/jLoven/hardness_test_area_detection/blob/master/matlab/indent_identifier.m), with code for determining the size of an imaged reticle at [https://github.com/jLoven/hardness\\_test\\_area\\_detection/blob/master/matlab/reticle\\_measurer.m](https://github.com/jLoven/hardness_test_area_detection/blob/master/matlab/reticle_measurer.m). The code for determining the size of an imaged reticle is identical to the aforementioned process for determining pixels per micron in AFM images. Given a metric for microns per pixel, the code for determining indent areas from metallized indents works by reducing image noise and then finding the area of the largest feature in an indent image. The user inputs the file path (any standard image file format is accepted in MATLAB's imread function) of a picture of an indent. First, the image is converted to grayscale. Then, the software performs a dilation with a square kernel of side length 4 pixels to reduce noise in the image. Then, an adaptive binarization with a sensitivity of 0.55 is performed to improve contrast and reduce noise. The software traces contours in the image using a Canny trace, and uses another adaptive binarization with a sensitivity of 0.4 to eliminate the noise of small contours. Finally, the software identifies the largest contour on the image, reports its size in square microns, and superimposes the pixels in the contour onto the original image in green.

The indent diagonal measurement code used for the analysis of CLSM masked images is also used for metallization images.

## VII. Acknowledgements

The author acknowledges NSF DMR-1120296 and Corning, Inc. for funding of this research. The author would also like to acknowledge Owen Lynch and Odell Dotson for assistance with image analysis methods, as well as Philip Carubia and Alison Rugar for guidance in sample metallization and Nicole Wiles and Shefford Baker for guidance and support.

## VIII. References

- [1] J. Petrík, P. Palfy. (2014). Variability of indentation size effect (ISE) of standard reference block. *29(1)*:43-50.
- [2] T. M. Gross, M. Tomozawa (2008). Fictive temperature-independent density and minimum indentation size effect in calcium aluminosilicate glass. *Journal of Applied Physics*, *104*(6):63529.
- [3] M. Zhao, W. S. Slaughter, M. Li, S. X. Mao (2003). Material-length-scale-controlled nanoindentation size effects due to strain-gradient plasticity. *Acta Materialia*, *51*(15): 4461-4469.
- [4] W. W. Gerberich, N. I. Tymiak, J. C. Grunlan, M. F. Horstemeyer, M. I. Baskes (2002). Interpretations of indentation size effects. *Journal of Applied Mechanics*, *69*(4):433-442.
- [5] I. Manika, J. Maniks (2006). Size effects in micro- and nanoscale indentation. *Acta Materialia*, *54*(8): 2049-2056.
- [6] T. M. Gross (2008). Glasses with fictive temperature-independent properties: minimization of indentation size effect and maximization of crack resistance. Rensselaer Polytechnic Institute.
- [7] H. Li, R. C. Bradt (1992). The indentation load size effect and the measurement of the hardness of vitreous silica. *Journal of Non-Crystalline Solids*, *146*(2-3):197-212.
- [8] G. D. Quinn, P. Green, K. Xu (2003). Cracking and the indentation size effect for Knoop hardness of glasses. *Journal of the American Ceramic Society*, *86*(3):441-448.
- [9] Smedskjaer, M.M. (2014). Indentation size effect and the plastic compressibility of glass. *Applied Physics Letters*, *104*(25):251906.
- [10] Quinn, G.D. (2005). Indentation Size Effect for Glasses: Yes, There is a Fracture Contribution. In *Fracture Mechanics of Ceramics*. 149–171.
- [11] T. Kavetskyy, J. Borc, K. Sangwal, V. Tsmots (2010). Indentation size effect and Vickers microhardness measurement of metal-modified arsenic chalcogenide glasses. *Journal of Optoelectronics and Advanced Materials*, *12*(10): 2082-209.
- [12] Oliver, W.C. & Pharr, G.M. (1992). An improved technique for determining hardness and elastic modulus using load and displacement sensing indentation experiments. *Journal of Materials Research*, *7*(6):1564-1583.

- [13] P. J. Blau (1986). Microindentation techniques in materials science and engineering. 889:95, 152.
- [14] K. Suganeswaran, N. Nithyavathy, Dr. R. Parameshwaran, G. Raja, M. Arun Prakash (2015). Hardness measurement using image analysis in Matlab. International Journal of Latest Trends in Engineering and Technology, 5(4): 288-297.
- [15] P. P. R. Filho, T. S. Cavalcante, V. H. C. de Albuquerque, J. M. R. S. Tavares (2010). Brinell and Vickers hardness measurement using image processing and analysis techniques. Journal of Testing and Evaluation, 38(1): 88-94.
- [16] V. B. Mendes, F. R. Leta (2003). Automatic measurement of Brinell and Vickers hardness using computer vision techniques. Proceedings, XVII IMEKO World Congress. 992-995.
- [17] Arora, A. et al. (1979). Indentation deformation/fracture of normal and anomalous glasses. Journal of Non-Crystalline Solids, 31(3):415–428.
- [18] Cook, R.F. & Pharr, G.M. (1990). Direct observation and analysis of indentation cracking in glasses and ceramics. Journal of the American Ceramic Society, 73(4):787–817.
- [19] Gross, T.M. & Tomozawa, M. (2008). Indentation-induced microhardness changes in glasses: Possible fictive temperature increase caused by plastic deformation. Journal of Non-Crystalline Solids, 354(34):4056–4062.
- [20] Gross, T.M., Tomozawa, M. & Koike (2009). A glass with high crack initiation load: Role of fictive temperature-independent mechanical properties. Journal of Non-Crystalline Solids, 355(9):563–568.
- [21] Limbach, R. et al. (2015). Plasticity, crack initiation and defect resistance in alkali-borosilicate glasses: From normal to anomalous behavior. Journal of Non-Crystalline Solids, 417–418:15–27.
- [22] Miura, T. et al. (2003). Universal hardness and elastic recovery in Vickers nanoindentation of copper phosphate and silicate glasses. Journal of the European Ceramic Society, 23(3):409–416.
- [23] Rouxel, T. et al. (2004). Indentation topometry in glasses by atomic force microscopy. Journal of Non-Crystalline Solids, 344(1-2):26–36.
- [24] Yoshida, S. et al. (2015). Direct observation of indentation deformation and cracking of silicate glasses. Journal of Materials Research, 30(15):2291–2299.

- [25] Yoshida, S., Sanglebœuf, J.-C. & Rouxel, T. (2005). Quantitative evaluation of indentation-induced densification in glass. *Journal of Materials Research*, 20(12):3404–3412.